Hawia, Sara, Goel, Saurav, Caro, Jaume, Bonet, Raül, Orrit-Prat, Jordi, Endrino, Jose L., Pearce, Oliver and Nishio, Wayne 2025. Antibacterial and osseointegration evaluation of silver ion implanted orthopaedic implants. Journal of Micromanufacturing

Publishers page:

Antibacterial and Osseointegration Evaluation of Silver Ion Implanted Orthopaedic Implants

Sara Hawi[a], Saurav Goel[b,c,d], Jaume Caro[e], Raül Bonet[e] and Jordi Orrit-Prat[e], Jose L Endrino[f], Oliver Pearce[g] and Wayne Nishio Ayre[h]*

[a] Cranfield University, Cranfield, MK43 0AL, UK

[b] China Beacons of Excellence Research and Innovation Institute (CBI), University of Nottingham Ningbo China (UNNC), Ningbo, 315101, China

[c] London South Bank University, 103 Borough Road, London, SE10 AA, UK

[d] University of Petroleum and Energy Studies, Dehradun, 248007, India

[e] Eurecat, Centre Tecnològic de Catalunya, Unit of Metallic and Ceramic Materials, Plaça de la Ciència 2, 08243 Manresa, Spain

[f] Universidad Loyola Andalucia, Av de las Universidades s/n, 41704 Dos Hermanas, Sevilla, Spain

[g] Milton Keynes University Hospital, Milton Keynes, MK6 5LD, UK

[h] Cardiff University, Cardiff, CF14 4XY, UK

*Corresponding Author E-mail: goeLs@Lsbu.ac.uk

22 **Abstract**

23 This study investigates the efficacy of silver ion-implanted or impregnated freeform

24 surfaces of Locking Compression Plates (LCPs) for orthopaedic applications,

25 specifically targeting the prevention of surgical site infections without affecting the

26 future removability of fracture fixation devices. Using stainless steel LCPs as a

27 testbed, we explored the antibacterial resistance of silver implanted LCP plates

28 against Staphylococcus aureus as well as assessed the biocompatibility through

29 osteoblast-like cell behaviour.

30 Silver ion implanted LCPs demonstrated a 72% reduction in bacterial adhesion

31 compared to controls ($p < 0.01$, Cohen's $d = 8.2$), along with a 4.5-fold increase in the

32 proportion of dead bacteria ($p < 0.001$, Cohen's $d = 10.6$), although this efficacy was

33 lower than that reported for similar ion dosages in the literature, likely due to the

34 complexities of non-planar geometries.

35 Furthermore, the silver-treated surfaces influenced osteoblast-like cells to exhibit a

36 >60% reduction in attachment compared to untreated controls, with cells showing

37 predominantly rounded morphology, an outcome beneficial for fracture fixation plates

38 intended for eventual removal, as it discourages osseointegration. Our findings

39 revealed the promising antimicrobial potential of silver ions as an excellent agent for

40 the improved antibacterial performance of the LCP surfaces for fracture fixation,

41 marking a departure from the traditional focus on permanent implant osseointegration.

42 A key novelty of this work is the application of silver ion implantation to full-scale,

43 geometrically complex orthopaedic implants, as opposed to the flat samples typically

44 used in prior studies. The observed discrepancies between our results on freeform

45 surfaces and theoretical predictions/experimental data from flat samples necessitate

46   a deeper investigation into the influence of complex surface geometries. These results

47   underscore the critical need to refine both our models and implantation processes to

48   account for the effects of complex surface topography.

49   **Keywords**: Antibacterial; Silver implantation; biotesting; Osseointegration

50

51   **1. Introduction**

52   Orthopaedic implants serve as artificial joint replacements and as plates and screws

53   for fracture fixation when natural joints and bone deteriorate or fail under mechanical

54   stress. However, not all implants necessitate osseointegration, such as forearm plates

55   that assist in fractured bone fixation [1], which makes infection control a higher priority.

56   However, as their surfaces inherently lack bactericidal properties, they often serve as

57   a breeding ground for bacterial adhesion, proliferation, and biofilm formation. This

58   leads to potential risks of infection and, occasionally, aseptic loosening due to poor

59   osseointegration, a problem observed especially in non-cemented implants [2]. In

60   orthopaedic care, the incidence of fracture-related infections presents a significant

61   challenge, with rates varying between 1.3% and 9% across different implant sites. This

62   variability highlights the complexities of managing infections in a field where outcomes

63   can be critically influenced by numerous factors. Illustratively, a study from one of

64   Europe's busiest trauma centers reported 330 infection episodes in 294 patients over

65   six years [3], underscoring the prevalence and the difficulty of infection control in high-

66   volume settings. Iliaens *et al.* [4] shed light on the economic burden, noting that the

67   direct costs associated with treating these infections are eight times higher than for

68   patients without infections. Additionally, they highlight the profound impact on quality

69   of life, with a marked decrease in physical function among those affected. The

70   cumulative effect of these issues emphasizes that the repercussions of fracture-

71 related infections extend far beyond financial costs, affecting patient health and well-

72 being deeply.

73 Traditional methods of preventing biomaterial-bound bacterial infections largely rely

74 on antibiotics. However, the rise of antibiotic resistance necessitates alternative

75 solutions. Researchers have focused on understanding bacterial adhesion and

76 developing surfaces that deter bacterial adhesion and growth. Incorporation of

77 antibacterial elements such as silver (Ag), copper (Cu), and zinc (Zn) have shown

78 promising results due to their ability to interact with bacterial cellular processes and

79 causing irreversible DNA damage to bacteria [5, 6].

80 Silver impregnation, because of its dual antibacterial and osteogenic properties [7] has

81 gained attention in both research and industrial applications [5]. Companies like

82 Accentus Medical Ltd have introduced products like Agluna®, that leverage silver's

83 antibacterial properties [6]. Despite the progress, these solutions still face challenges

84 with implementation, especially concerning osseointegration [8, 9], largely due to

85 issues like coating delamination. Therefore, alternative methods like ion implantation

86 are being explored.

87 Ion implantation is a sophisticated surface engineering technique that utilizes ionized

88 atomic species accelerated at high energy in a vacuum environment. This method

89 serves as a means of immobilization of accelerated particles into the surface of a

90 substrate. Unlike conventional surface coatings, this process enables the atoms to

91 penetrate the substrate at the sub-surface level. This unique characteristic eliminates

92 the risk of delamination; an issue often encountered with traditional surface coatings.

93 It also allows for the preservation of the substrate's bulk properties [10], making it

94 advantageous for a variety of applications.

95   Among the various ion implantation methods, Plasma Immersion Ion Implantation

96   (PIII) is particularly noteworthy [11-16]. It stands out for its versatility and effectiveness

97   in modifying surfaces with complex geometries, eliminating the line-of-sight

98   restrictions seen in other implantation techniques. PIII operates in a specialized

99   vacuum chamber, equipped with a workpiece stage, plasma source, and high-voltage

100 pulse modulator [17]. During the process, the samples are submerged in high-density

101 plasma and subjected to a high-voltage negative pulse, facilitating the ion

102 bombardment towards the substrate surface. This results in a thin, implanted sublayer

103 typically in the order of tens of nanometers.

104 This technique can be further tailored by adjusting the implantation parameters to

105 control ion concentration and depth, offering exceptional control over the modified

106 layer. Moreover, PIII can be used in conjunction with different plasma ion sources like

107 Metal Vapor Vacuum Arc (MEVVA), Electron Cyclotron Resonance (ECR), and

108 Kaufman among others [17]. One particularly exciting application is the implantation

109 of biocidal elements like Ag, Cu, or Zn, which can be used for the creation of

110 antibacterial surfaces. PIII even allows the integration of these biocidal elements with

111 bioactive ones such as Ca and Mg, paving the way for more comprehensive

112 biomedical applications.

113 Given these advantages and the level of control offered by PIII, it opens a new frontier

114 in the creation of antibacterial biomaterials. While the incorporation of antimicrobial

115 agents into various medical products is not novel, what is relatively new is the surface

116 engineering of biomaterials themselves to imbue them with antibacterial properties.

117 Although antimicrobial materials have long been used in disinfecting solutions and

118 wound dressings [18, 19], their incorporation into the very surfaces of biomedical

119   implants has recently gained considerable attention. Among these, silver and silver

120   nanoparticles (Ag NPs) stand out. They are increasingly being employed due to their

121   high reactivity and expansive active surface area. Under environmental and

122   physiological conditions, Ag NPs oxidize and release Ag^+ ions, which are theorized to

123   be the hub of the bactericidal action of silver by disrupting bacterial membranes and

124   reducing their viability [20-22]. This happens through strong interactions between the

125   ionic Ag^+ and thiol groups of cystine residues of proteins present in bacteria cell walls

126   [24]. While higher dosages of implanted Ag have been shown to yield greater

127   bactericidal effects [17, 20], recent research highlights the importance of optimizing

128   the concentration of silver to achieve antibacterial activity without cytotoxic effects [23].

129   This balance is particularly relevant for Ag ion-implanted substrates, which have also

130   demonstrated favorable outcomes in osseointegration and cytocompatibility [24].

131   *Staphylococcus aureus (S. aureus)* is of particular interest in this work as it is an

132   opportunistic pathogen associated with the majority of orthopaedic surgical site

133   infections, community and hospital-acquired infections [25, 26].

134   This research focuses on the chemical modification of orthopaedic biomedical

135   surfaces, specifically LCPs. It explores the potential of ion implantation, which is

136   emerging as a promising avenue to tackle bacterial infections related to orthopaedic

137   applications.

138   While the existing body of literature robustly demonstrates the efficacy of silver ion

139   implantation in enhancing antibacterial properties, a significant limitation persists: the

140   vast majority of these studies are conducted on flat, polished coupons of implant

141   materials [24, 27]. This approach, while valuable for foundational research, fails to

142   capture the challenges and realities of treating commercial orthopaedic devices, which

143 feature intricate screws holes, curvatures, and non-line-of-sight surfaces. Therefore,

144 the primary novelty of this research lies in its focus on applying silver Plasma

145 Immersion Ion Implantation to full-scale, commercial Locking Compression Plates

146 (LCPs) with complex freeform geometries. This work bridges the gap between

147 idealized laboratory studies and real-world clinical application, critically evaluating how

148 complex topography influences antibacterial efficacy and cellular response.

149 In the subsequent sections, a comparative analysis is provided between unmodified

150 LCP samples and those subjected to silver ion implantation. A significant novelty of

151 this research lies in the application of these techniques to full-scale orthopaedic

152 implants, a perspective currently underrepresented in the literature. The study

153 scrutinizes the effects of silver ion implantation on bacterial attachment, cell

154 morphology, and overall antibacterial performance, aiming to yield valuable insights

155 about the effectiveness of this promising approach in real-world settings.

156 **2. Methods**

157

158 *2.1. Silver Ion Implantation*

159

160 Stryker orthopaedic (Michigan, US) implant samples, including LCPs composed of

161 stainless steel, spiral blades composed of titanium aluminum niobium alloy and the

162 femoral component of a knee replacement implant composed of cobalt-chromium alloy

163 (Figure 1) acquired from Milton Keynes University Hospital (MKUH) were

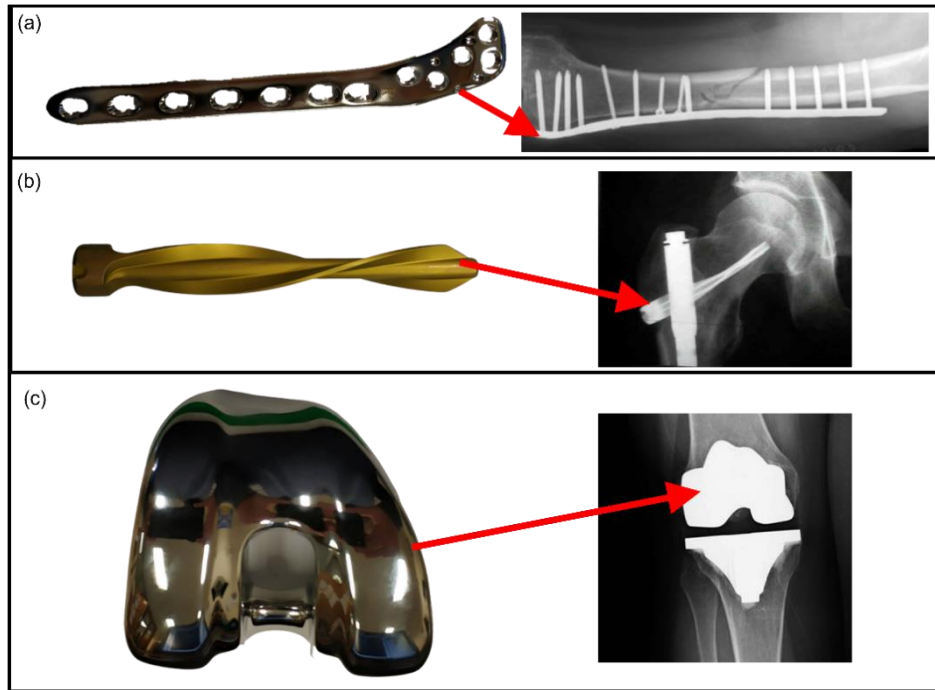164 subsequently processed with silver ion implantation.

165

Figure 1: (a) Locking Compression Plate (stainless steel) and its application [28], (b) spiral blade (titanium niobium alloy) and its application [29] and (c) knee replacement femoral component (cobalt chromium alloy) and its application [30].

Silver implantation processes for orthopaedic implant parts were performed in a pulsed filtered cathodic vacuum arc system (PFCVA-450, Plasma Technology Limited, Hong Kong). To reduce the incorporation of detrimental microparticles into the samples, this system is equipped with two pulsed filtered cathodic arc sources, where the generated arc plasmas are directed into the vacuum chamber by an electromagnetic field applied to the curved ducts. The samples were positioned in the center of the chamber (240 mm away from the exit of the filtered duct), and they were negatively biased to a high pulsed voltage. More details of this equipment can be found elsewhere [31]. A schematic and picture of the system are presented in figure 2.

The implantation parameters, including ion dose, energy and substrate temperature, were guided by the review of the existing literature to achieve a surface concentration of silver that is biocidal yet minimizes potential cytotoxic effects [23, 24]. A dose of

181 approximately 4.0×10^{17} ions/cm² was targeted since this range has been previously

182 shown to confer significant antibacterial properties against *S. aureus* on metallic

183 substrates without completely inhibiting mammalian cell function [24, 32]. An

184 implantation energy of -20 kV was selected to ensure sufficient ion penetration into the

185 sub-surface region (tens of nanometers, as confirmed by Stopping and Range of Ions

186 in Matter (SRIM) simulations shown later in Fig. 4), creating a durable reservoir of

187 silver ions that is less susceptible to wear than a superficial coating [10]. A substrate

188 temperature of 175°C was maintained to facilitate the diffusion and incorporation of

189 implanted ions without inducing undesirable phase transformations or thermal stress

190 in the stainless-steel substrate, which has a much higher annealing temperature [10].

191 Two high-purity silver cathodes (99.95 %) were co-evaporated on a rotating sample.

192 The cathodes were ignited at 50 V, using a pulse duration of 450 µs at a frequency of

193 7 Hz, generating a mean arc current of about 0.17 A. An argon flow of 2 sccm was

194 introduced through each arc source. The implantation process was carried out at a

195 working pressure of 0.03 Pa, for 60 min and at 175 ºC substrate temperature. The

196 samples were biased to a pulsed potential of -20 kV (7 Hz, 600 µs). Under these

197 conditions, the bias current was ~34 mA, corresponding to an ion dose of

198 approximately 4.0×10^{17} ions/cm².

199

200 (a)

201

202 (b)
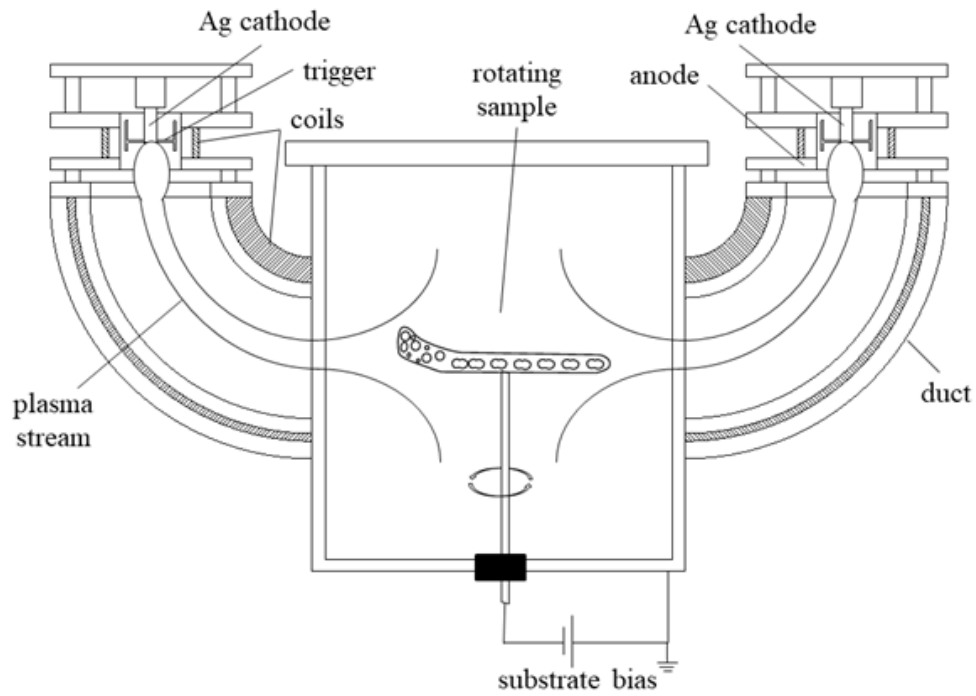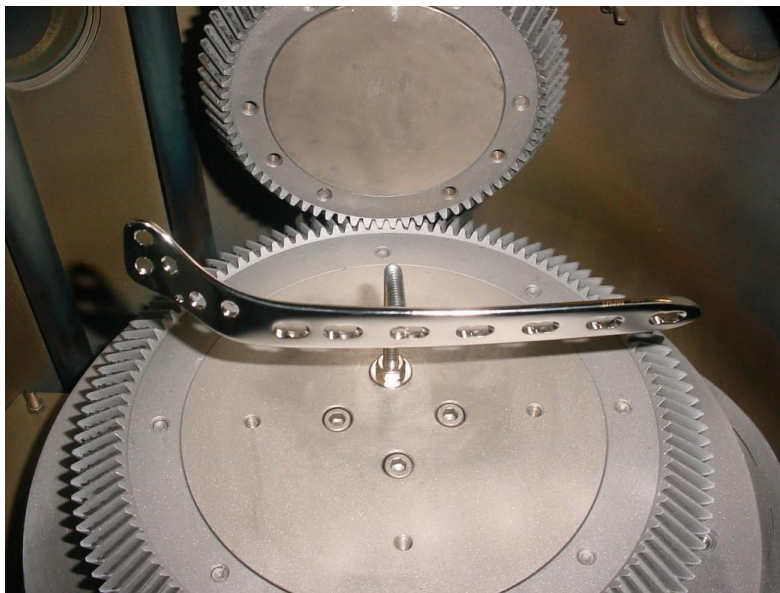
203 Figure 2 (a) Schematic of the pulsed filtered cathodic vacuum arc system. (b)

204 Placement of the Locking Compression Plate (LCP) prosthesis on the rotating sample

205 holder.

206   All fabricated samples were cleaned by sonication with acetone for 15 min, sonication

207   with isopropanol for 10 min and then immersed in 70% ethanol (for around 2 min) in a

208   24 well plate. The successful implantation of silver was functionally validated by the

209   significant antibacterial effects described in the Results section. Direct surface

210   chemical analysis on these specific, complex-geometry implants was not feasible with

211   our available equipment; this presents a valuable direction for future research using

212   advanced, tailored characterization techniques. The samples were then transferred to

213   a fresh well plate and allowed air dry before characterisation and biological evaluation.

214   *2.2 Bacterial Growth*

215   Before each bacterial attachment experiment, *S. aureus* NCTC 7791 (Culture

216   Collections, UK Health Security Agency, UK) bacterial cultures were prepared from a

217   single colony on tryptone soya agar (TSA) and grown overnight in tryptone soya broth

218   (TSB) at 37 °C, 5 % CO_2.

219   Overnight bacterial culture (10 mL) was transferred to a universal container and

220   centrifuged at 5000 g for 5 min. The bacterial pellet was then resuspended with

221   phosphate buffered saline (PBS) and centrifuged again at 5000 g for 5 min. The pellet

222   was resuspended in PBS to an optical density (OD600 nm) of 0.09 (corresponding to

223   approximately 1 x 10^7 CFU/ml).

224   *2.3 Bacterial Retention Study*
225

226   The LCP specimen exhibits intricate geometrical characteristics, including multiple

227   surface curvatures. In alignment with established engineering methodologies that

228   advocate preliminary coupon testing, regions with minimal surface curvature were

229   identified and segmented into 0.5 x 0.5 cm subcomponents. These subcomponents

230   were subsequently bisected to create stable base sections, thereby ensuring that the

231   treated surface would face upward.

232   A 15 µl droplet of the inoculum was added to each sample surface in a 24-well plate

233   and incubated for 1 hour at 37 °C, 5% CO_2. The samples were then transferred to a

234   fresh 24-well plate and washed in 1 mL of 0.85% NaCl. Live/dead staining was

235   performed according to the manufacturer's instructions (LIVE/DEAD BacLight Viability

236   Kit, Thermofisher Scientific, UK) and imaged using an AX-70 fluorescent microscope

237   (Olympus, Japan) at magnifications of x10, x20 and x40. The percentage area

238   coverage or bacterial coverage (BC) was quantified using the ImageJ software as

239   outlined in a previous publication [33] from the x10 magnification images to ensure the

240   largest sample surface area was analyzed. Due to the complex topography of the LCP

241   samples, it was necessary to analyze multiple representative in-focus regions per

242   sample. While this provides a robust estimate, we acknowledge that techniques such

243   as confocal laser scanning microscopy, which can construct a 3D image from optical

244   sections, would provide a more comprehensive and accurate quantification for future

245   studies on such geometries.

246   *2.4 Osteoblast-like Cell Culture, attachment and morphology*

247

248   To assess the biocompatibility/cytotoxicity of the manufactured surfaces, human MG-

249   63 osteoblast-like cells (Sigma Aldrich, UK) were used. Cell attachment was studied

250   to determine how chemical modification might affect bone formation, and cell

251   morphology was studied to determine whether surface chemical modification may

252   induce cytoskeletal changes and therefore influence osteogenic potential. Cells

253   (passages 29–32) were seeded at 5000 cells/cm^2 and maintained in T75 cell culture

254   flasks in culture medium comprising of alpha minimum essential medium (α-MEM)

12

255 supplemented with 10 % (v/v) heat-inactivated fetal bovine serum (FBS) and

256 100 units/mL penicillin G sodium, 0.1 μg/mL streptomycin sulphate and 0.25 μg/mL

257 amphotericin (Thermofisher Scientific, UK). The cells were incubated at 37 $^{\circ}$C, 5 %

258 CO_2 and the medium were changed every 2–3 days. Cells were cultured until they

259 reached approximately 80 to 90% confluency before being used for subsequent

260 experiments.

261 The cells were detached using trypsin-EDTA, counted and seeded directly on the

262 control surfaces and the Ag ion implanted surfaces in a 24-well plate at a density of

263 100 cells/μl (approximately 1500 cells per sample). Samples were incubated for 1 h at

264 37 °C, 5 % CO_2 to allow attachment. The wells were then flooded with 500 μl of

265 complete culture media and incubated for a further 24 hours.

266 Subsequently, the samples were washed three times with PBS to remove non-

267 adherent cells and incubated in 500 μl of 10 % formalin overnight at 4 °C to fix the

268 attached cells. Following incubation, the formalin solution was removed, and the

269 samples were washed three times with tris-buffered saline (TBS). The cells were then

270 permeabilized with filtered 1 % Triton X-100 (Sigma Aldrich, UK) for 30 min at room

271 temperature. After permeabilization, the samples were washed three times with TBS.

272 Incubation of the samples for 1 hour at room temperature with a solution of 1 % bovine

273 serum albumin (Vector Laboratories, UK) in TBS was performed to block non-specific

274 binding sites. Following incubation, the actin filaments of the cells were stained with

275 freshly prepared fluorescein isothiocyanate (FITC) labelled phalloidin (diluted 1:50 in

276 TBS, Sigma Aldrich, UK) and incubated in the dark for 40 mins at room temperature.

277 The samples were then washed three times with TBS and allowed to air dry for 5 min.

278 Subsequently,10 μl of 4′,6-diamidino-2-phenylindole (DAPI, Vector Laboratories, UK)

279 was added to each sample surface to stain the nuclei of the cells. Images of the cell

280   actin filament and nuclei were taken at magnifications of x10, x20, x40 using an AX70

281   Olympus fluorescent microscope (Olympus, Japan). FITC and DAPI channels were

282   superimposed using ImageJ. Cell attachment and morphology analysis were

283   performed on fluorescent images.

284   Similar to the bacterial quantification, cell attachment analysis on these freeform

285   surfaces was challenged by topography. The qualitative assessment of morphology

286   and relative attachment is clear; however, precise quantitative analysis would be

287   enhanced in future work by using 3D surface scanning to normalize counts to actual

288   surface area or by using z-stack imaging via confocal microscopy.

289   *2.5 Surface Preparation for SEM Bacteria Imaging*
290

291   Following bacterial tests for silver-implanted surfaces, the adhered bacteria were fixed

292   in 10 % formalin for 10 min to fix the attached bacteria while retaining their

293   morphologies through protein crosslinking. After that, they were rinsed and dried again

294   for 1 hour, then placed in different concentrations of ethanol for 10 min successively

295   (30 %, 50 %, 70 %, 90 % and 100 %) and dried in a class 2 flow hood [8, 34]. Following

296   submersion in ethanol, the samples were sputter-coated with a 10 nm gold layer to

297   ensure conductivity for SEM imaging. A Tescan S8215G field emission (Tescan,

298   Czechia) scanning electron microscope (FE-SEM) was employed for the visualization.

299   *2.6. Statistical analysis*
300

301   Bacterial and cell culture experiments were performed in triplicate for all surfaces.

302   Three images (x10) were taken at random and analyzed for each sample.

303   All data were first assessed for normality using the Shapiro–Wilk test. For normally

304   distributed datasets, one-way analysis of variance (ANOVA) was performed. Where

305   ANOVA indicated statistical significance ($p \leq 0.05$), Tukey's multiple comparison test

306   was applied for post-hoc pairwise comparisons. Data are presented as mean ±

307   standard deviation. Effect sizes (Cohen's *d*) were calculated where relevant to quantify

308   the magnitude of observed differences. A p-value of ≤ 0.05 was considered significant,

309   whereas in the case of a p-value of > 0.05, the results were reported as observational.

310   In the case that the ANOVA-obtained p-value was found to be less than 0.05, Tukey's

311   multiple comparisons test was performed to obtain pairwise comparisons between

312   data means. GraphPad Prism (Boston, USA) was used for the analysis. All data were

313   expressed as the mean accompanied by the standard deviation. For statistically

314   significant results ($p \leq 0.05$), the effect size was calculated using Cohen's d to quantify

315   the magnitude of the difference between groups.

316   **3. Results**

317   Silver ion surface treatment was conducted on three different types of implants, each

318   having a different material composition as outlined in the methods section. The

319   implants are shown before and after the surface treatment in Figure 3. Focusing on

320   fracture fixation applications, the scope of the experimental investigation was confined

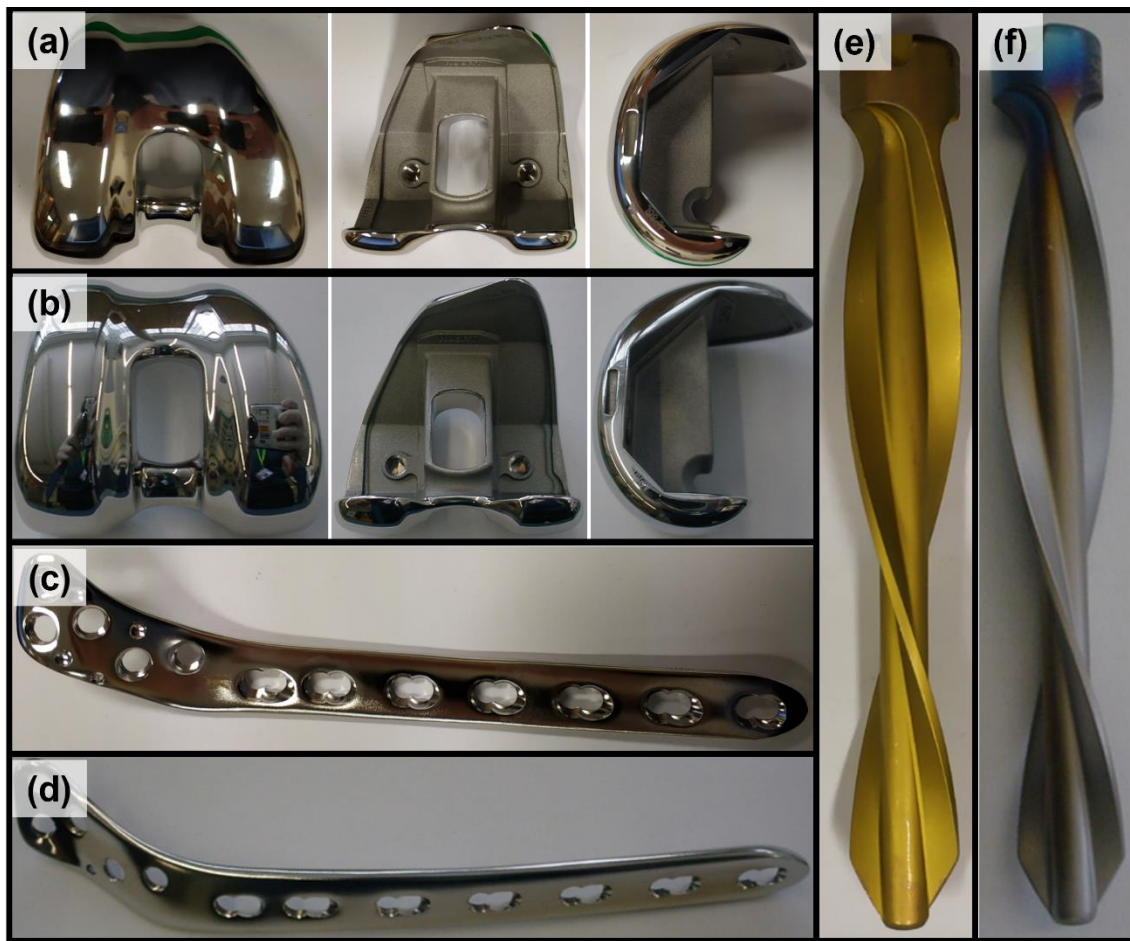321   to stainless steel LCP samples.

322

323 Figure 3: Knee replacement femoral component (a) before and (b) after surface

324 treatment. Locking Compression Plate (c) before and (d) after surface treatment.

325 Spiral blade (e) before and (f) after surface treatment.

326

327 It was not possible in this instance to conduct detailed and high-resolution chemical

328 analysis of these surfaces. However, the Stopping Range of Ions in Matter (SRIM)

329 simulations [35] were applied in order to gain insights into the depth of implantation of

330 silver in the bulk stainless-steel material of the LCP samples.

331 It must be emphasized that SRIM simulations represent an idealised model assuming

332 flat, homogeneous substrates and normal incidence ion trajectories. These

333   assumptions inherently limit their predictive power when applied to full-scale

334   orthopaedic implants with freeform geometries.

335
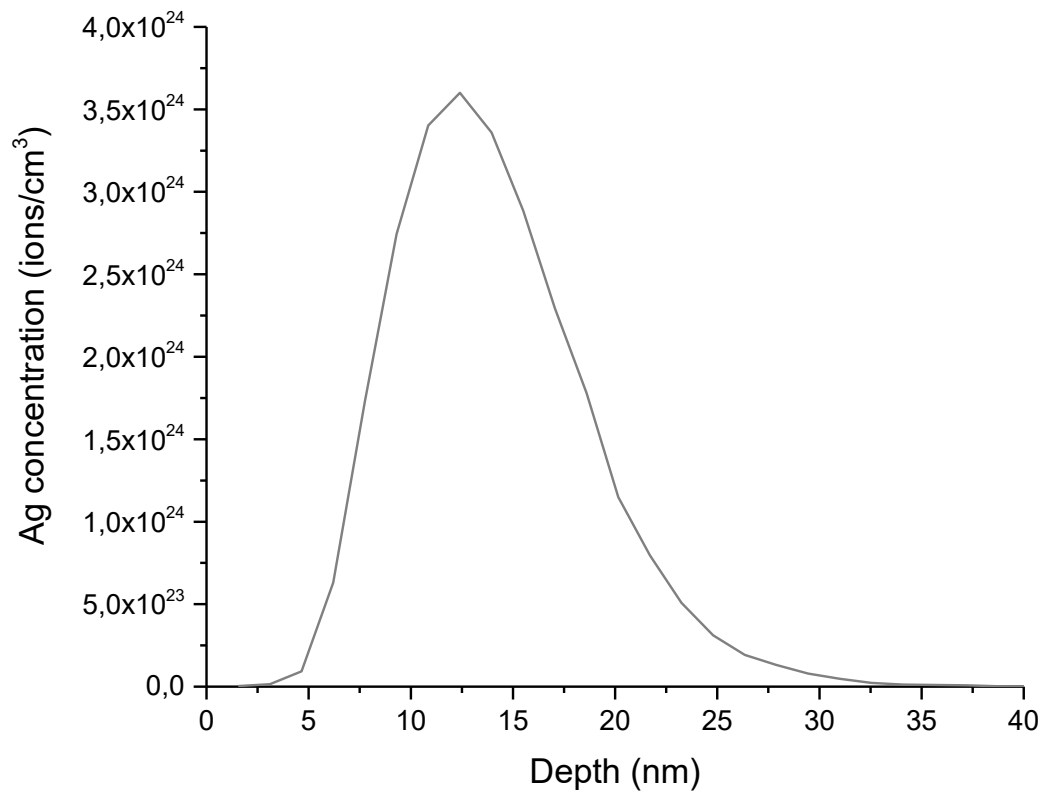
336   Figure 4: SRIM-simulated silver ion concentration versus implantation depth in
337   stainless steel. The curve represents an idealised depth profile generated under
338   assumptions of flat geometry, normal ion incidence and homogeneous material
339   composition. These results should be interpreted as a theoretical reference; real
340   freeform implant geometries may deviate substantially due to angular incidence,
341   shadowing, and surface roughness effects. Direct experimental characterisation is
342   required in future work to validate these distributions.

343

344   The SRIM simulation graph in Figure 4 demonstrates a distinct profile of silver ion

345   concentration as a function of implantation depth in stainless steel. The concentration

346   of silver ions exhibits a peak at a depth of 13 nm beneath the implant surface,

347   indicating the maximum penetration of ions achieved through the implantation

348   process. Beyond this peak, the concentration decreases gradually, suggesting a

17

349   diffusion-controlled penetration of silver ions into the stainless-steel substrate with the

350   presence of silver at a maximum depth of 33 nm.

351   SEM micrographs in Figure 5 (a, b) show fewer S. aureus cells attached to Ag-treated

352   LCPs compared to controls. Representative fluorescence micrographs illustrating the

353   antibacterial efficacy and cellular response are presented in Figure 5 (c,d,e,f). These

354   micrographs provided a clear visual corroboration of the quantitative data. Live/Dead

355   staining showed dense bacterial biofilms on control surfaces, contrasted by sparse,

356   predominantly dead colonies on Ag-treated implants shown in Fig. 5 (c,d).

357   Furthermore, staining of MG-63 cells revealed healthy, spread morphologies on

358   controls, while Ag-treated surfaces exhibited significantly fewer cells with a rounded,

359   non-adherent morphology Fig. 5 (e,f). Also, the number of cells attached to the

360   untreated stainless steel implant surface was higher than the number of cells attached

361   to the Ag-treated surfaces. Additionally, the cells seem to be presenting a healthier

362   morphology and attachment to the untreated surfaces compared to the Ag-treated
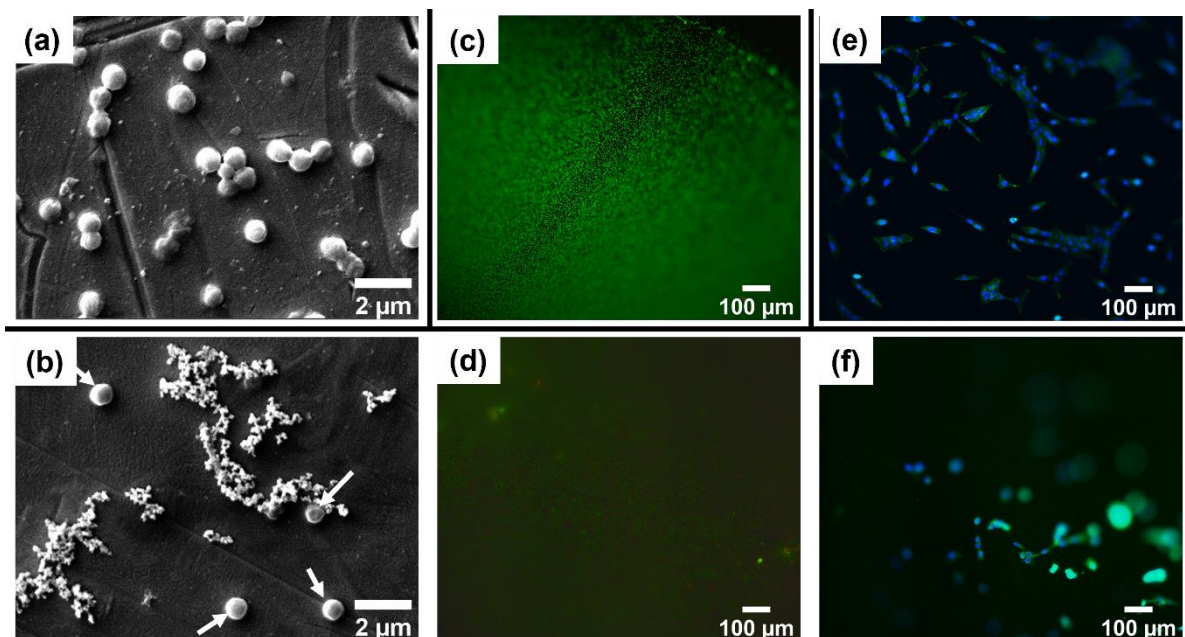
363   surfaces.

364
365

Figure 1: **Scanning Electron Microscope (SEM) images of S. aureus on (a) control and (b) silver-treated LCP samples. White arrows indicate attached bacteria. Fluorescence microscopy images of S. aureus (Live/Dead stain) on (c) control and (d) silver-treated LCP samples. Fluorescence microscopy images of MG-63 osteoblast-like cells (Phalloidin/DAPI stain) on (e) control and (f) silver-treated LCP samples.**

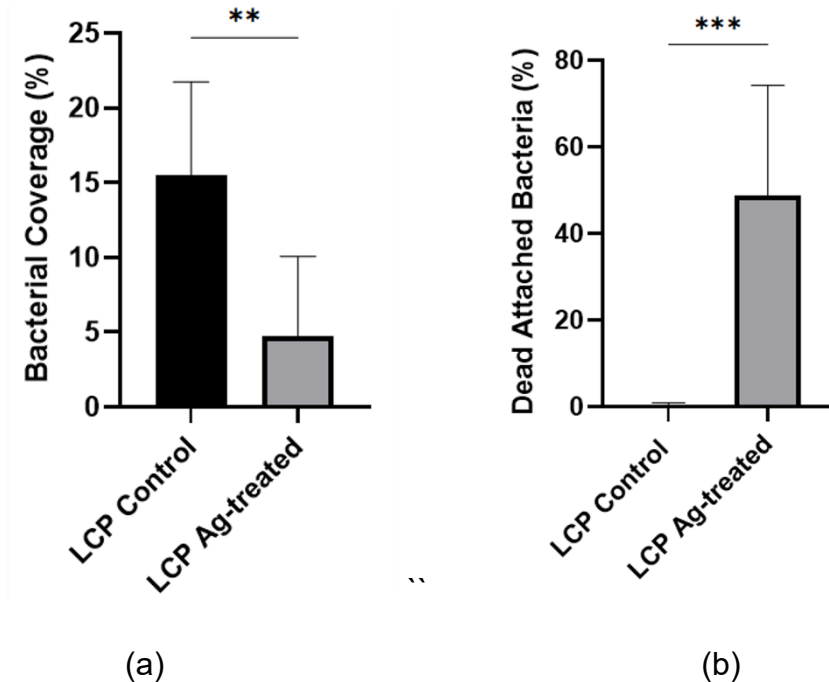(a)   (b)

Figure 6: (a) The bacterial coverage on both LCP control and Ag-treated samples (b) The percentage of dead bacteria attached to the surface of LCP control and Ag-treated samples. Statistical significance was determined using one-way ANOVA with Tukey's post-hoc test. **$p < 0.01$, ***$p < 0.001$. The calculated Cohen's d effect sizes for the differences are 8.2 and 10.6, respectively, indicating an extremely large magnitude of effect.

The silver-treated LCP samples showed a significantly reduced bacterial coverage compared to the control LCP ($p < 0.01$, Cohen's *d* = 8.2), while the percentage of dead bacteria was significantly higher on the Ag-treated surfaces ($p < 0.001$, Cohen's *d* = 10.6) (Figure 6). These very large effect sizes indicate a substantial and meaningful biological effect of the silver treatment.

4. Discussion

389   The SRIM simulations indicate variations in silver ion distribution within the stainless-

390   steel orthopaedic implants, especially when considering the unique challenges

391   presented by freeform surfaces. Unlike the uniform distribution expected in theoretical

392   models or simulations tailored for flat surfaces, the intricate geometries of the tested

393   implants suggest a more complex implantation dynamic. This complexity is particularly

394   evident in the context of surface treatments aimed at enhancing antibacterial

395   properties through silver ion implantation. The simulations predict a heterogeneous

396   distribution of silver ions, which might not directly correlate with a uniform

397   enhancement of antibacterial efficiency across the entire surface of the implants.

398   Although the SRIM results provide valuable insights into the potential distribution of

399   silver ions, the actual antimicrobial efficacy of these treated surfaces would likely be

400   influenced by the specific surface geometries and the resulting variation in ion

401   concentration at different locations.

402   In this study, the SRIM simulations were conducted by feeding the software details

403   about the composition of the target material, in this case, the LCP material, the ion

404   energy, the implanted/impregnated material (silver) and the angle of incidence (normal

405   incidence).

406   A limitation of this study on full-scale implants is the lack of direct surface chemical

407   characterization (e.g., XPS, TOF-SIMS) to quantify the silver concentration, depth

408   profile and chemical state. As noted, this was due to the significant technical challenge

409   of analyzing large, non-planar and intricately shaped objects with standard surface

410   science equipment, which is typically designed for flat, small coupons. Consequently,

411   we relied on SRIM simulations for a theoretical depth profile and, most importantly, on

412   functional biological assays to confirm the implantation's efficacy. The significant

413   antibacterial results shown in Figure 6 provide strong indirect evidence that silver was

414 successfully implanted and is biologically active. The observed discrepancy between

415 our results and the literature for flat samples underscores the fact that without direct

416 characterisation, it is difficult to deconvolute the precise effect of geometry on the ionic

417 distribution. Therefore, we explicitly state that future work must prioritise overcoming

418 these characterization hurdles, potentially through the use of destructively sectioning

419 implants or developing new analytical protocols for complex shapes, to directly link

420 implantation parameters on freeform surfaces to biological outcomes.

421 The decreased bacterial attachment could be an indication that silver ions actively kill

422 bacteria in the solution, decreasing the number of live bacteria seeking attachment. It

423 has indeed been documented that Ag-ion implantation acts better on free-floating

424 bacteria, as in this state, the Ag^+ ions can easily interact with the bacteria [36]. A key

425 methodological challenge in this study was the accurate quantification of biological

426 response on the complex freeform surfaces of the clinical implants. Standard

427 epifluorescence microscopy, used here, has a limited depth of field, meaning only

428 portions of the curved LCP surface could be in focus at one time. This required

429 analysis of multiple representatives in focus regions, a method which, while providing

430 a good estimate, introduces potential for selection bias and may under-represent the

431 total surface area. Advanced techniques such as confocal laser scanning microscopy

432 (which can compile z-stacks into a 3D image) or 3D surface profilometry (to map

433 topography and correct fluorescence counts for real surface area) would provide

434 superior quantification. Despite this limitation, the qualitative results are unequivocal:

435 a stark contrast in bacterial coverage and cell density is visually apparent between Ag-

436 treated and control surfaces across all replicates. The quantitative data presented,

437 therefore, should be interpreted as a robust *relative comparison* between treatment

438 groups, rather than an absolute measure of total coverage.

439   Beyond the antibacterial efficacy, a key finding of this study is the observed reduction

440   in osteoblast-like cell (MG-63) attachment and spreading on the silver-treated

441   surfaces, as evidenced by their rounded morphology (Figure 5f). This has important

442   and nuanced clinical implications for implant stability and healing. For permanent

443   implants, such as joint arthroplasties, this would be a significant concern, as strong

444   osseointegration is essential for long-term stability and load-bearing function.

445   However, the context of the implant's purpose is critical. Locking Compression Plates

446   (LCPs) and other fracture fixation devices are primarily temporary implants, designed

447   to provide mechanical support only until the bone has healed, after which they are

448   often removed. In this specific application, the clinical paradigm is different. Excessive

449   osseointegration is a well-documented complication, making removal surgery difficult,

450   requiring extensive dissection, and increasing the risk of re-fracture, operative time,

451   and patient morbidity.

452   Therefore, the observed inhibition of osteoblast function, while a drawback for

453   permanent implants, can be reinterpreted as a potential *benefit* for temporary fracture

454   fixation devices. A surface that actively resists strong bone ingrowth could significantly

455   simplify future removal procedures. This positions silver ion implantation not as a

456   universal coating, but as a promising strategy for a specific implant class where the

457   primary clinical challenges are infection prevention and the facilitation of easier

458   removal, without completely sacrificing the mechanical stability required for the initial

459   healing period. Future studies should aim to quantify this balance between sufficient

460   stability for healing and reduced integration for removal.
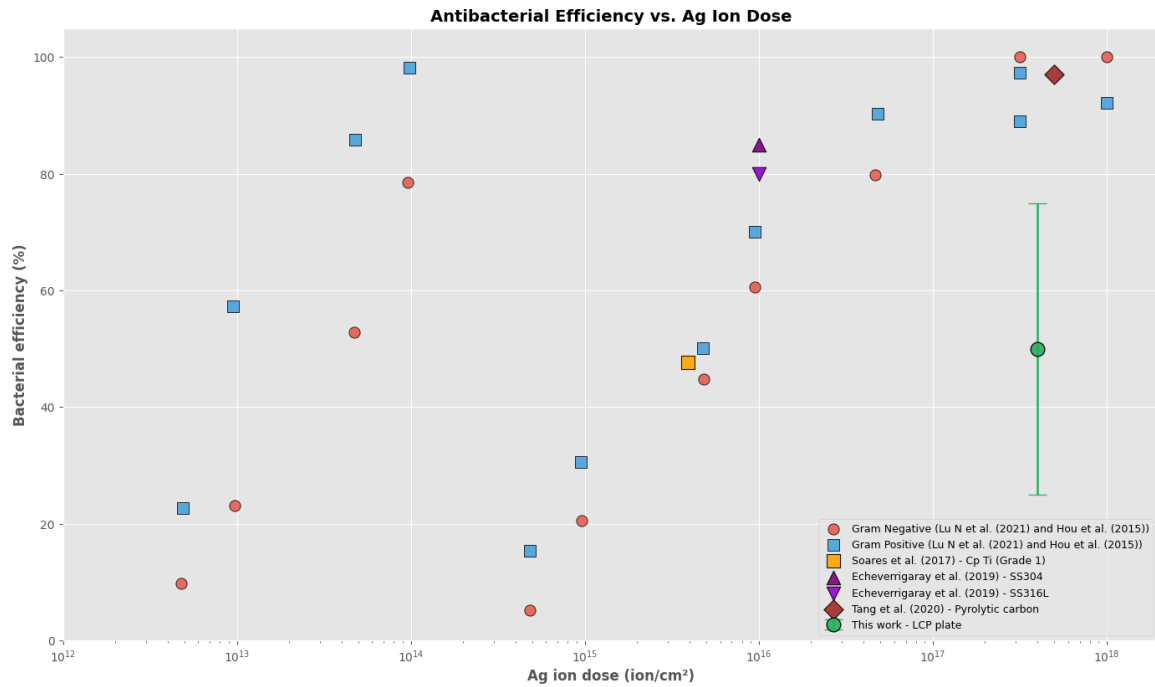
461

Figure 7: The position of the current results within the literature. The significantly lower antibacterial efficacy observed in this study, compared to literature values for flat coupons treated with a similar nominal dose, is attributed to the reduction in effective dose caused by the complex geometry of the freeform LCP implant. Data for the plot were extracted from several sources [32, 37-40].

As illustrated in Figure 7, the mean antibacterial efficacy of the Ag-treated LCP surfaces in this study is significantly lower than the efficiencies reported in the literature for a similar nominal Ag ion dosage [32, 37-40]. This can be quantitatively explained by the complex geometry of the implant. The reduction in efficacy is attributed to two primary geometric effects:

a. Surface Area Shadowing: A commercial LCP is not a flat surface but a complex structure with numerous screw holes, edges, and curved regions. During the PIII process, these features create zones of "self-shielding" where the ion flux is partially or completely blocked. A simple geometric model of our

23

477   LCP plate estimates that approximately 20-30% of the total surface area

478   consists of these shielded regions (e.g., the walls of screw holes), which would

479   receive a substantially lower ion dose.

480   **b. Angular Dependence of Implanted Dose:** Ion implantation is most effective

481   at normal incidence (0°). The effective implanted dose decreases as a function

482   of the angle of incidence (θ) relative to the surface normal, following the

483   relation D_eff = D_nominal × cos(θ). On a complex geometry like an LCP, a

484   significant portion of the surface is oriented at high angles. For example, a

485   surface at 60° incidence would receive an effective dose of only 50% of the

486   nominal dose (cos(60°) = 0.5), leading to a sub-lethal silver concentration.

487   Therefore, the nominal dose (4.0×10^{17} ions/cm²) represents a maximum value

488   only achievable on ideal flat surfaces oriented perpendicular to the ion flux.

489   The effective weighted average dose across the entire implant is considerably

490   lower due to shadowing and angular effects. This model robustly explains the

491   discrepancy with flat-sample studies and underscores that process parameters

492   must be optimized for the specific geometry of the target implant to ensure a

493   uniformly bactericidal surface.

494   This divergence is a central finding and is attributed to the fundamental difference in

495   substrate geometry. The cited studies utilised flat, polished samples, which allow for

496   uniform ion flux and predictable implantation profiles. In contrast, our work on freeform

497   LCP surfaces reveals that complex geometries lead to varied angles of incidence and

498   potential shadowing effects, resulting in a non-uniform distribution of implanted silver

499   ions. This heterogeneity likely explains the observed reduction in overall antibacterial

500   performance compared to idealized flat surfaces.

501 The distinction in antibacterial efficiency between the implants studied and those

502 reported in literature for similar Ag ion dosages draws attention to the impact of surface

503 geometry on treatment effectiveness. The expected ion concentration and distribution

504 on freeform surfaces such as LCP may differ from those on flat samples, potentially

505 explaining the variations in observed antimicrobial performance. This discrepancy

506 suggests that the specific conditions and characteristics of the implantation process,

507 as well as the surface to be treated, play crucial roles in determining the final

508 antibacterial efficacy of silver-ion-implanted/impregnated surfaces.

5. Conclusions

510 This study investigated the application of silver ion implantation on full-scale

511 orthopaedic Locking Compression Plate implants to explore its potential for

512 antimicrobial activity against *S. aureus*. Our experimental findings showed a

513 statistically significant 72% reduction in bacterial attachment and a 4.5-fold increase

514 in dead bacteria on silver-impregnated surfaces, compared to controls. Additionally,

515 osteoblast attachment was reduced by over 60%, indicating that while antimicrobial

516 properties are enhanced, osseointegration is correspondingly suppressed.

517 This study demonstrates that the antibacterial performance of silver ion implantation,

518 previously established on flat samples, is significantly challenged by the complex

519 geometries of real-world orthopaedic implants. The observed deviations from results

520 on flat surfaces are not simply experimental error but are a direct consequence of

521 freeform topography. Therefore, the primary conclusion of this work is that optimisation

522 of surface engineering techniques such as Plasma Immersion Ion Implantation (PIII)

523 must be conducted on clinically relevant geometries to be truly predictive of clinical

524 performance.

25

525   The difference between the results obtained for flat surfaces from existing literature

526   and the freeform surfaces in this study highlighted the need for further research and

527   optimization of the implantation process on intricate surfaces. This need is also

528   coupled with the requirement for in-depth chemical analysis of surfaces to determine

529   implantation depth and concentration more accurately.

530   Moreover, the study observed a reduction in osteoblast cell attachment and spreading

531   on silver-treated surfaces. This outcome suggests that while silver ion implantation

532   may enhance antimicrobial properties, it could also influence osseointegration

533   processes. Notably, this reduction in osteoblast activity may facilitate future removal

534   of the implants, given that certain orthopaedic fixtures, including LCPs, are intended

535   for eventual extraction after fulfilling their temporary role in supporting bone healing.

536   This study also underscored the significant challenges in imaging and quantifying

537   biological data on freeform surfaces using traditional microscopy. Future work must

538   adopt the reviewer's excellent suggestion to employ advanced methodologies such as

539   confocal laser scanning microscopy and 3D surface scanning to overcome the

540   limitations of depth of field and to normalize data to the true surface area, thereby

541   enabling absolute quantification on complex implant geometries.

542   In summary, while the promising antibacterial activity of silver-ion-treated surfaces was

543   evidenced, future work must overcome the challenges of surface chemical analysis on

544   complex geometries (e.g., via destructive cross-sectioning and analysis of

545   representative areas) to precisely quantify silver concentration and distribution. This

546   will allow for the adaptation and optimisation of implantation strategies for freeform

547   surfaces to fully exploit the potential of silver ion implantation in orthopaedic

548   applications. These findings highlight the need to tailor surface micromanufacturing

549 approaches specifically for temporary fracture fixation implants, where both infection

550 control and ease of removal are critical clinical requirements.

551

560 **References:**

561 [1] N. Anantavorasakul, Lans J., Wolvetang N.H., Walbeehm E.T., Chen N., Forearm Plate
562 Fixation: Should Plates Be Removed?, The Archives of Bone and Joint Surgery 10(2) (2022) 153.
563 [2] A. Katzer, Loehr J., Early loosening of hip replacements: causes, course and diagnosis,
564 Journal of Orthopaedics Traumatology 4 (2003) 105-116.
565 [3] K.H. Patel, Gill L.I., Tissingh E.K., Galanis A., Hadjihannas I., Iliadis A.D., Heidari N., Cherian
566 B., Rosmarin C., Vris A.J.A., Microbiological Profile of Fracture Related Infection at a UK Major
567 Trauma Centre, 12(9) (2023) 1358.
568 [4] J. Iliaens, Onsea J., Hoekstra H., Nijs S., Peetermans W.E., Metsemakers W.-J., Fracture-
569 related infection in long bone fractures: a comprehensive analysis of the economic impact and
570 influence on quality of life, Injury 52(11) (2021) 3344-3349.
571 [5] X. Chen, Schluesener H.J., Nanosilver: a nanoproduct in medical application, J Toxicology
572 letters 176(1) (2008) 1-12.
573 [6] H. Wafa, Grimer R., Reddy K., Jeys L., Abudu A., Carter S., Tillman R., Retrospective
574 evaluation of the incidence of early periprosthetic infection with silver-treated endoprostheses
575 in high-risk patients: case-control study, The bone joint journal 97(2) (2015) 252-257.
576 [7] G. Jin, Qin H., Cao H., Qian S., Zhao Y., Peng X., Zhang X., Liu X., Chu P.K., Synergistic effects
577 of dual Zn/Ag ion implantation in osteogenic activity and antibacterial ability of titanium,
578 Biomaterials 35(27) (2014) 7699-7713.
579 [8] S. Hawi, Goel S., Kumar V., Giusca C., Pearce O., Ayre W.N., Precision Laser Manufacturing
580 and Metrology of Nature-Inspired Bioactive Surfaces for Antibacterial Medical Implants,
581 Surfaces and Interfaces 62 (2025) 106267.
582 [9] S. Hawi, Goel S., Kumar V., Pearce O., Ayre W.N., Ivanova E.P., Critical review of nanopillar-
583 based mechanobactericidal systems, ACS Applied Nano Materials 5(1) (2022) 1-17.

584 [10] J.K. Hirvonen, Treatise on Materials Science and Technology: Ion Implantation, Academic
585 press1980.
586 [11] F. Kroner, Schork R., Frey L., Burenkov A., Ryssel H., Phosphorus ion shower implantation
587 for special power IC applications, 2000 International Conference on Ion Implantation
588 Technology Proceedings. Ion Implantation Technology-2000 (Cat. No. 00EX432), IEEE, 2000, pp.
589 476-479.
590 [12] J.R. Conrad, Radtke J.L., Dodd R.A., Worzala F.J., Tran N.C., Plasma source ion-implantation
591 technique for surface modification of materials, Journal of Applied Physics 62(11) (1987) 4591-
592 4596.
593 [13] A. Anders, From plasma immersion ion implantation to deposition: a historical perspective
594 on principles and trends, Surface and Coatings Technology 156(1-3) (2002) 3-12.
595 [14] J. Matsuo, Aoki T., Seki T., Cluster Ion Implantation-Prospects and Challenges, 2007
596 International Workshop on Junction Technology, IEEE, 2007, pp. 53-54.
597 [15] Y. Gotoh, Tsuji H., Ishikawa J., Molecular ion implanter equipped with liquid-metal alloy ion
598 source, Review of Scientific Instruments 71(2) (2000) 780-782.
599 [16] D. Gupta, Plasma immersion ion implantation (PIII) process-physics and technology, Int. J.
600 Adv. Technol 2(4) (2011) 471-490.
601 [17] M. Larrañaga-Altuna, Zabala A., Llavori I., Pearce O., Nguyen D.T., Caro J., Mescheder H.,
602 Endrino J.L., Goel G., Ayre W.N., Seenivasagam R.K., Tripathy D.K., Armstrong J., Goel S.,
603 Bactericidal surfaces: An emerging 21st-century ultra-precision manufacturing and materials
604 puzzle, Applied Physics Reviews 8(2) (2021) 021303.
605 [18] A.C. Miller, Rashid R.M., Falzon L., Elamin E.M., Zehtabchi S., Silver sulfadiazine for the
606 treatment of partial-thickness burns and venous stasis ulcers, Journal of the American
607 Academy of Dermatology 66(5) (2012) e159-e165.
608 [19] L.P. Arendsen, Thakar R., Sultan A.H., The use of copper as an antimicrobial agent in health
609 care, including obstetrics and gynecology, Clinical microbiology reviews 32(4) (2019)
610 10.1128/cmr. 00125-18.
611 [20] S. Lopez, Hallali N., Lalatonne Y., Hillion A., Antunes J.C., Serhan N., Clerc P., Fourmy D.,
612 Motte L., Carrey J., Magneto-mechanical destruction of cancer-associated fibroblasts using
613 ultra-small iron oxide nanoparticles and low frequency rotating magnetic fields, Nanoscale
614 Advances 4(2) (2022) 421-436.
615 [21] S. Kirthika, Goel G., Matthews A., Goel S., Review of the untapped potentials of
616 antimicrobial materials in the construction sector, Progress in Materials Science 133 (2023)
617 101065.
618 [22] S.A. Ahmad, Das S.S., Khatoon A., Ansari M.T., Afzal M., Hasnain M.S., Nayak A.K.,
619 Bactericidal activity of silver nanoparticles: A mechanistic review, Materials science for energy
620 technologies 3 (2020) 756-769.
621 [23] J. Orrit-Prat, Bonet R., Rupérez E., Punset M., Ortiz-Hernández M., Guillem-Marti J., Lousa
622 A., Cano D., Díaz C., Fuentes G.G., Bactericidal silver-doped DLC coatings obtained by pulsed
623 filtered cathodic arc co-deposition, Surface and Coatings Technology 411 (2021) 126977.
624 [24] H. Qin, Cao H., Zhao Y., Jin G., Cheng M., Wang J., Jiang Y., An Z., Zhang X., Liu X.,
625 Antimicrobial and osteogenic properties of silver-ion-implanted stainless steel, ACS applied
626 materials & interfaces 7(20) (2015) 10785-10794.
627 [25] M. Ribeiro, Monteiro F.J., Ferraz M.P., Infection of orthopedic implants with emphasis on
628 bacterial adhesion process and techniques used in studying bacterial-material interactions,
629 Biomatter 2(4) (2012) 176-194.
630 [26] G. Pietrocola, Campoccia D., Motta C., Montanaro L., Arciola C.R., Speziale P., Colonization
631 and infection of indwelling medical devices by Staphylococcus aureus with an emphasis on
632 orthopedic implants, International journal of molecular sciences 23(11) (2022) 5958.

633 [27] S. Mei, Wang H., Wang W., Tong L., Pan H., Ruan C., Ma Q., Liu M., Yang H., Zhang L., Cheng
634 Y., Zhang Y., Zhao L., Chu P.K., Antibacterial effects and biocompatibility of titanium surfaces
635 with graded silver incorporation in titania nanotubes, Biomaterials 35(14) (2014) 4255-4265.
636 [28] D.S. Kim, Kim Y.M., Choi E.S., Shon H.C., Park K.J., Cho B.K., Park J.K., Lee H.C., Hong K.H.,
637 Repeated metal breakage in a femoral shaft fracture with lateral bowing-a case report, Journal
638 of the Korean Fracture Society 25(2) (2012) 136-141.
639 [29] https://www.wheelessonline.com/joints/spiral-blade/ accessed on, (2.9.25).
640 [30] M.R. Angerame, Jennings J.M., Holst D.C., Dennis D.A., Management of bone defects in
641 revision total knee arthroplasty with use of a stepped, porous-coated metaphyseal sleeve, JBJS
642 Essential Surgical Techniques 9(2) (2019) e14.
643 [31] A. Pardo, Buijnsters J.G., Endrino J.L., Gómez-Aleixandre C., Abrasonis G., Bonet R., Caro J.,
644 Effect of the metal concentration on the structural, mechanical and tribological properties of
645 self-organized aC: Cu hard nanocomposite coatings, Applied surface science 280 (2013) 791-
646 798.
647 [32] H. Tang, Liu T., Liu X., Gu H., Zhao J., A study on biocompatibility and bactericidal properties
648 of pyrolytic carbon by silver ion implantation, Nuclear Instruments and Methods in Physics
649 Research Section B: Beam Interactions with Materials and Atoms 255(2) (2007) 304-308.
650 [33] W.N. Ayre, Scott T., Hallam K., Blom A.W., Denyer S., Bone H.K., Mansell J.P.,
651 Fluorophosphonate-functionalised titanium via a pre-adsorbed alkane phosphonic acid: A
652 novel dual action surface finish for bone regenerative applications, Journal of Materials Science:
653 Materials in Medicine 27 (2016) 1-12.
654 [34] F.H. Rajab, Liauw C.M., Benson P.S., Li L., Whitehead K.A., Picosecond laser treatment
655 production of hierarchical structured stainless steel to reduce bacterial fouling, Food and
656 bioproducts processing 109 (2018) 29-40.
657 [35] J.F. Ziegler, Biersack J.P., The stopping and range of ions in matter, Treatise on heavy-ion
658 science: volume 6: astrophysics, chemistry, and condensed matter, Springer1985, pp. 93-129.
659 [36] I. Sukhorukova, Sheveyko A., Shvindina N., Denisenko E., Ignatov S., Shtansky D.,
660 Approaches for controlled Ag+ ion release: influence of surface topography, roughness, and
661 bactericide content, ACS Applied Materials & Interfaces 9(4) (2017) 4259-4271.
662 [37] X. Hou, Mao D., Ma H., Ai Y., Zhao X., Deng J., Li D., Liao B., Antibacterial ability of Ag–TiO2
663 nanotubes prepared by ion implantation and anodic oxidation, Materials Letters 161 (2015) 309-
664 312.
665 [38] N. Lu, Chen Z., Zhang W., Yang G., Liu Q., Böttger R., Zhou S., Liu Y., Effect of silver ion
666 implantation on antibacterial ability of polyethylene food packing films, Food Packaging and
667 Shelf Life 28 (2021) 100650.
668 [39] T.P. Soares, Garcia C.S.C., Roesch-Ely M., Maia da Costa M.E.H., Giovanela M., Aguzzoli C.,
669 Cytotoxicity and antibacterial efficacy of silver deposited onto titanium plates by low-energy ion
670 implantation, Journal of Materials Research 33(17) (2018) 2545-2553.
671 [40] F.G. Echeverrigaray, Echeverrigaray S., Delamare A.P.L., Wanke C.H., Figueroa C.A.,
672 Baumvol I.J.R., Aguzzoli C., Antibacterial properties obtained by low-energy silver implantation
673 in stainless steel surfaces, Surface and Coatings Technology 307 (2016) 345-351.

674